

# Electroviscous Effects in Low Reynolds Number Flow through a Microfluidic Contraction with Rectangular Cross-Section

Malcolm R Davidson, Ram P. Bharti, Petar Liovic, and Dalton J.E. Harvie

**Abstract**—The electrokinetic flow resistance (electroviscous effect) is predicted for steady state, pressure-driven liquid flow at low Reynolds number in a microfluidic contraction of rectangular cross-section. Calculations of the three dimensional flow are performed in parallel using a finite volume numerical method. The channel walls are assumed to carry a uniform charge density and the liquid is taken to be a symmetric 1:1 electrolyte. Predictions are presented for a single set of flow and electrokinetic parameters. It is shown that the magnitude of the streaming potential gradient and the charge density of counter-ions in the liquid is greater than that in corresponding two-dimensional slit-like contraction geometry. The apparent viscosity is found to be very close to the value for a rectangular channel of uniform cross-section at the chosen Reynolds number ( $Re = 0.1$ ). It is speculated that the apparent viscosity for the contraction geometry will increase as the Reynolds number is reduced.

**Keywords**—Contraction, Electroviscous, Microfluidic, Numerical.

## I. INTRODUCTION

UNDERSTANDING flows in micrometer-sized channels is necessary for the development of new microfluidic devices with the ability to transport and manipulate liquids at very small scales for new and existing biotechnology applications [1]. In recent years there has been an explosion of research activity related to microfluidic and micro-scale devices [2].

At micrometer scales, surface phenomena such as surface tension and electrokinetic effects assume increased importance [3]-[4]. Electrokinetic phenomena develop in a channel containing an ionic liquid when the channel walls in contact with the liquid are charged. Counter-ions in the liquid are attracted to a charged wall and a diffuse electrical double layer (EDL) forms in which the concentration of counter-ions decreases away from the wall. The EDL thickness can vary from nanometers to one or two micrometers, depending on the ionic concentration and electrical properties of the liquid [5]. In pressure-driven flow the counter-ions are advected downstream. This creates a current that generates a

(streaming) potential field. This potential induces an electrokinetic force that opposes the fluid flow, increasing the flow resistance and the apparent viscosity (electroviscous effect) [5]-[6].

Studies that model the electroviscous effect are usually applied to channels with uniform cross-section and include slit-like channels [7]-[9], and channels with cross-sections that are cylindrical [10]-[11], elliptic [12], and rectangular [13]-[14]. However, many microfluidic elements such as T-junctions and contractions have non-uniform geometries. Recently, the authors performed numerical studies of the electroviscous effect in a 4:1:4 contraction-expansion for slit-like [15]-[16] and cylindrical [17] geometries. Flow in these geometries is two-dimensional in character. However, microchannels are typically constructed to have rectangular cross-sections so that the flow in corresponding contraction-expansions is three-dimensional. This paper presents numerical predictions of the electroviscous effect in a 4:1:4 contraction-expansion geometry having a rectangular cross-section, for a particular choice of electrokinetic and flow parameters. The aim is to compare the electroviscous effect in that case with predictions for a corresponding slit-like (planar) geometry.

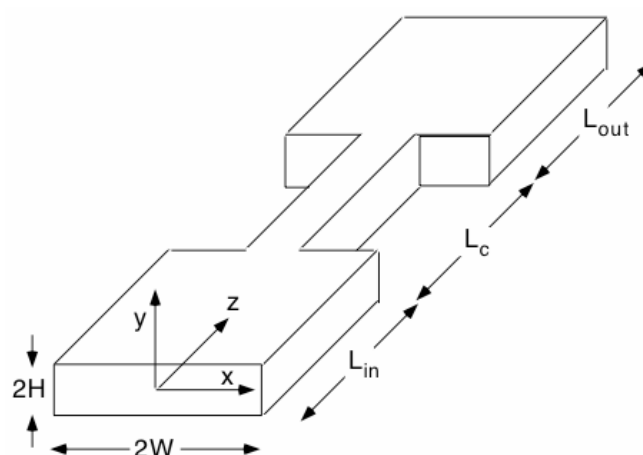


Fig. 1 Schematic of the contraction-expansion flow geometry

All authors are with the Department of Chemical and Biomolecular Engineering, The University of Melbourne, Australia (e-mail: m.davidson@unimelb.edu.au, prakashr@unimelb.edu.au, pliovic@unimelb.edu.au, daltonh@unimelb.edu.au).

## II. MODEL DESCRIPTION

We investigate the three-dimensional flow of an ionic liquid through a 4:1:4 contraction-expansion of rectangular cross-section as shown in Fig. 1. The liquid is taken to be a 1:1 electrolyte solution of constant viscosity ( $\mu$ ) and density ( $\rho$ ). Thus the anions and cations (specified by + and -, respectively) are assumed to have equal valences  $z = 1$ . They are also assumed to have equal diffusivities  $D$ .

The cross-sections of the inlet and outlet sections (width  $2W$  and depth  $2H$ ) are taken to be equal with  $H/W = 0.25$ . For this aspect ratio, the cross-section of the contracted section is a square of side  $2H$ . A net immobile electrostatic charge of surface density  $\sigma$  is assumed on the channel walls. The bulk ionic concentration of each species and the mean inflow velocity are denoted by  $n_0$  and  $\bar{V}$ , respectively.

### A. Governing Equations

The equations governing the flow, the electric field, and ion transport are rendered dimensionless by scaling the velocity, length, time, number density of anions and cations, and electrical potential by  $\bar{V}$ ,  $W$ ,  $W/\bar{V}$ ,  $n_0$ ,  $kT/ze$ , respectively. Here  $e$  is the elementary charge,  $k$  is the Boltzmann constant, and  $T$  denotes temperature. The dimensionless equations are

$$\nabla^2 U = -\frac{1}{2} K^2 (n_+ - n_-) \quad (1)$$

$$\frac{\partial n_+}{\partial t} + \nabla \cdot (\mathbf{v} n_+) = \frac{1}{\text{ReSc}} \left[ \nabla^2 n_+ + \nabla \cdot (n_+ \nabla U) \right] \quad (2)$$

$$\frac{\partial n_-}{\partial t} + \nabla \cdot (\mathbf{v} n_-) = \frac{1}{\text{ReSc}} \left[ \nabla^2 n_- - \nabla \cdot (n_- \nabla U) \right] \quad (3)$$

$$\frac{\partial \mathbf{v}}{\partial t} + \nabla \cdot (\mathbf{v} \mathbf{v}) = -\nabla P + \frac{1}{\text{Re}} \nabla \cdot \left[ \nabla \mathbf{v} + (\nabla \mathbf{v})^T \right] - \frac{BK^2}{\text{Re}^2} (n_+ - n_-) \nabla U \quad (4)$$

$$\nabla \cdot \mathbf{v} = 0 \quad (5)$$

where (1) is the Poisson equation relating the total electrical potential  $U$  at a point to the charge density there, (2)-(3) are the Nernst-Planck equations describing conservation of each ion species in terms of the number of positive ( $n_+$ ) and negative ( $n_-$ ) ions per unit volume, and (4)-(5) are the usual Navier-Stokes equations, but with an extra (electrical) force in the momentum equation due to free charges.

The dimensionless groups in (1)-(4) are

$$\text{Re} = \frac{\rho \bar{V} W}{\mu}, \quad \text{Sc} = \frac{\mu}{\rho D}, \quad B = \frac{\rho k T^2 \epsilon_0 \epsilon}{2z^2 e^2 \mu^2}, \quad K^2 = \frac{2z^2 e^2 n_0 W^2}{\epsilon_0 \epsilon k T} \quad (6)$$

where  $\text{Re}$  and  $\text{Sc}$  are the Reynolds and Schmidt numbers, respectively, and  $K$  is the dimensionless inverse Debye length which is a measure of the ratio of the channel half-width  $W$

to the EDL thickness. The parameter  $B$  is fixed for a given liquid at a specified temperature.

### B. Boundary Conditions

Since the channel walls have electrostatic charge, there is a jump in the dielectric displacement normal to the boundary between the liquid and the wall material. The magnitude of this jump equals the surface charge density. Here we ignore the dielectric displacement in the wall material since most liquids in biotechnology are aqueous-based, and water has a dielectric constant of about 80 compared with approximately 3 for typical materials used for manufacturing microchannels. In that case, the boundary condition at the wall for the electrical potential is

$$\frac{\partial U}{\partial n_w} = S \quad (7)$$

in dimensionless form, where  $n_w$  is the outwards normal to the channel wall and  $S$  is the non-dimensional surface charge density given by

$$S = \frac{ze\sigma W}{\epsilon_0 \epsilon k T} \quad (8)$$

The other wall boundary conditions are zero total flux of each ion species normal to the wall and the no-slip velocity condition.

The inlet conditions for velocity and ion concentration are imposed from the solution for steady, fully developed electroviscous flow in a uniform channel having the same rectangular cross-section as the inlet. This solution is obtained by a finite difference procedure, the details of which will be presented elsewhere. (Semi-analytical methods can also be used [14].) The longitudinal potential gradient at the inlet is determined by specifying zero net current there. The corresponding potential gradient at the outlet is taken to be uniform over the cross-section and is chosen to satisfy Gauss's law over the flow domain. At steady state, the current passing through the outlet cross-section also becomes zero. The other outlet conditions are zero longitudinal gradients of the normal velocity and ion concentrations, and a longitudinal pressure gradient chosen to ensure global mass conservation.

## III. NUMERICAL METHOD

The authors have adapted a single-phase version of the transient two-fluid finite volume method of Rudman [18] to include electrokinetics, and use this to calculate a steady state solution. We use this approach because we have already used the Rudman algorithm extensively for transient droplet deformation in non-electrokinetic flows [19], and we plan to extend the adapted code in the future to study transient droplet flows with electrokinetics included. Calculations are performed in parallel using 32 processors on a uniform staggered grid with 32 mesh cells spanning the half-width  $W$

of the inlet, and  $\delta x = \delta y = \delta z$ . The code structure for parallel processing has been adapted from parallel code developed by the third author for other applications [20]. Since the system has two planes of symmetry, only one quadrant of the channel cross-section needs to be considered.

A procedure is implemented to increase the rate of approach to steady state by permitting time steps that are larger than the viscous time step limit in the explicit Rudman algorithm. (This limit is very small for low Reynolds numbers, as is considered here.) The time step is then only limited by numerical stability constraints involving the electrokinetic parameters as well as the Courant condition, as described by Davidson and Harvie [15]. The above-mentioned procedure at each time step is to repeatedly perform the viscous update to the momentum equation over a number of smaller time steps that are each less than the viscous limit before performing the more time consuming solution of the Poisson equation for the pressure correction.

#### IV. RESULTS AND DISCUSSION

We present results for  $B = 2.34 \times 10^{-4}$ ,  $Sc = 1000$ ,  $Re = 0.1$ ,  $K = 4$  and  $S = 8$ . The first two parameters are derived using the properties of water and a temperature of 298 K. The chosen values of scaled inverse Debye length  $K$  and dimensionless surface charge density  $S$  are intermediate in the range considered previously by the authors [15], [17], and show a significant EDL. Although the surface charge is taken to be positive ( $S > 0$ ), results for the corresponding negative value can be obtained by setting new values of  $U$ ,  $n_+$  and  $n_-$  equal to  $-U$ ,  $n_-$  and  $n_+$ , respectively. Calculations for a full range of parameter values in an expansion-contraction with rectangular cross-section are deferred for a later paper. The geometry is chosen with  $L_m/W = L_c/W = L_{out}/W = 5$  (see Fig. 1).

Fig. 2 shows the dimensionless charge distribution ( $n_+ - n_-$ ) in the mid-plane  $y = 0$  compared with the charge distribution in the corresponding slit-like geometry. As expected, the negative charge in the EDL, induced by the positive surface charge, decreases away from the wall. However, the magnitude of the EDL charge is greater in the three dimensional (3D) rectangular geometry, and the EDL is thicker, than it is in the slit-like geometry. This occurs because wall surface area per unit length along the channel is less for the slit, in which case the surface charge, and hence the charge in the EDL, is of lower magnitude in the slit. The variation in the charge along the central  $z$ -axis shown in Fig. 3 is consistent with Fig. 2, with the charge being more negative for the 3D rectangular geometry. Note that Fig. 3 shows that the length of slit outlet section is not long enough at the Reynolds number ( $Re = 0.1$ ) to achieve fully developed conditions at the exit, whereas [15] shows that it is long enough when  $Re = 0.01$ . In contrast, fully developed conditions at the exit are achieved here for  $Re = 0.1$  in the 3D rectangular geometry.

Fig. 4 compares the distribution of dimensionless total electrical potential in the mid-plane  $y = 0$  with the potential distribution in a corresponding slit-like geometry. In both cases, the potential decreases in the direction of flow because of the advection of negative charge along the channel. The magnitude of the potential gradient ensures that the net current is zero. It is greater for the 3D rectangular geometry because more counter-ions are exposed to the flow as shown in Figs. 2 and 3. The variation of the potential in the inlet, contraction and outlet sections is quantified more clearly in Fig. 5 which shows the potential on the central  $z$ -axis. The potential drop over each section is greater for the 3D rectangular geometry than it is for the 2D slit, consistent with Fig. 4.

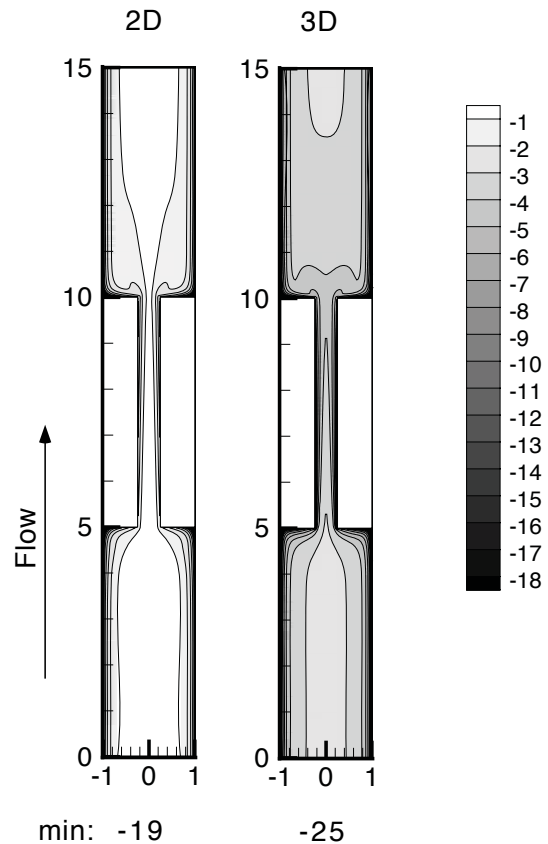


Fig. 2 Dimensionless charge distribution in the mid-plane  $y = 0$  (3D rectangular) compared with the corresponding charge distribution in a slit-like expansion-contraction (2D)

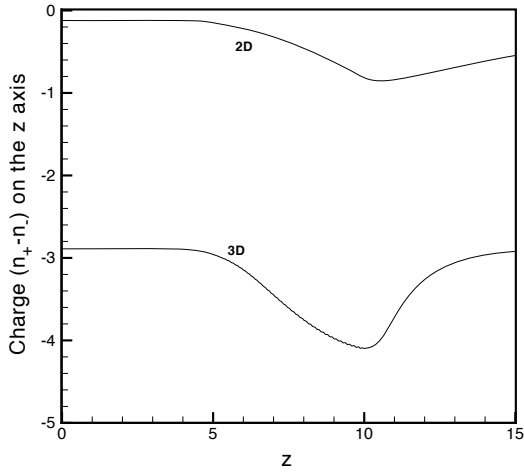


Fig. 3 Dimensionless charge on the central  $z$ -axis (3D rectangular) compared with that for a corresponding slit-like expansion-contraction (2D)

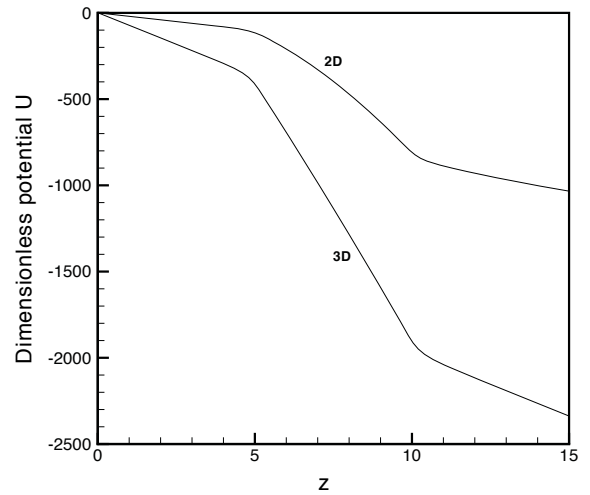


Fig. 5 Dimensionless total potential on the central  $z$ -axis (3D rectangular) compared with that for a corresponding slit-like expansion-contraction (2D)

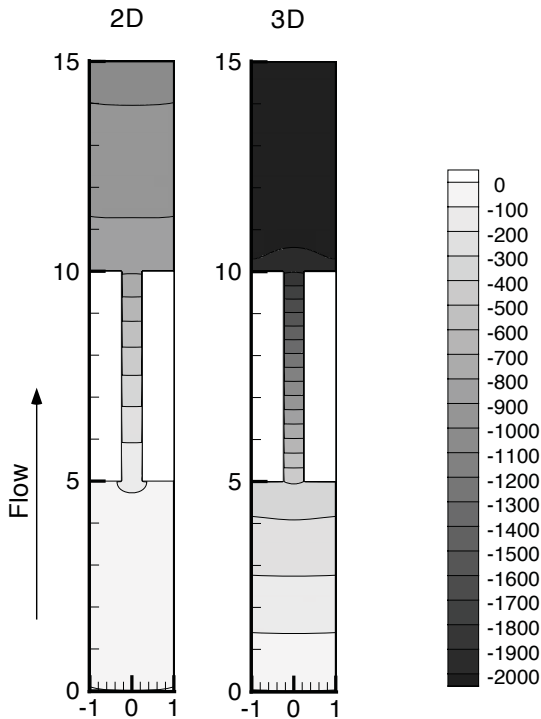


Fig. 4 Distribution of dimensionless total electrical potential in the mid-plane  $y = 0$  (3D rectangular) compared with the corresponding potential distribution in a slit-like expansion-contraction (2D)

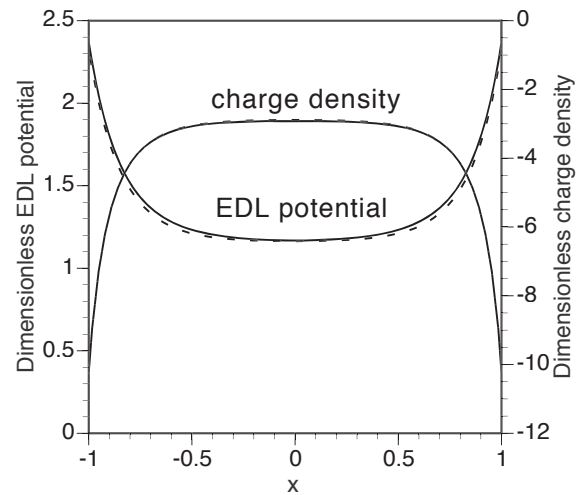


Fig. 6 Variation of dimensionless EDL potential and charge with  $x$  for  $y = 0$  on the outlet cross-section of the rectangular expansion-contraction channel (solid lines). The dashed lines are profiles for a uniform rectangular channel

In Fig. 6 the lateral profiles of electrical potential and charge density on the  $x$ -axis in the cross-section at the channel exit ( $z_{exit} = L_{in} + L_c + L_{out}$ ) are compared with those for fully developed conditions in a uniform channel having the same cross-section. The potential  $U$  is modified as  $U(x, y, z_{exit}) - U(0, 0, z_{exit}) + \psi(0, 0)$  and compared with  $\psi(x, y)$  which is the EDL potential over the cross-section of a uniform channel obtained from a finite difference solution. The modification has the effect of removing the longitudinal variation in  $U$  and forcing the value of the modified potential to equal  $\psi(0, 0)$  on the central  $z$ -axis. Fig. 6 makes the comparison along the  $x$ -axis ( $y = 0$ ), showing that the results are almost coincident as is expected when fully developed conditions are achieved at

the exit. The corresponding profiles of charge density are also coincident. The same degree of correspondence is found along the  $y$ -axis of the outlet plane and in contour plots over the cross-section, but these are not shown.

#### A. Apparent Viscosity

The electrical force in the momentum equation (4) causes an additional flow resistance manifested by a pressure drop  $\Delta P$  that is larger than the pressure drop  $\Delta P_0$  that occurs when there is no electrical force for the same flow rate. This effect can be quantified using an apparent viscosity  $\mu_{\text{eff}}$  that is the viscosity required with no electrical forcing to achieve the pressure drop  $\Delta P$  for the given flow rate. For steady flow at low Reynolds number,

$$\mu_{\text{eff}} / \mu = \Delta P / \Delta P_0 \quad (9)$$

where  $\mu$  is the physical viscosity. The Reynolds number used here ( $\text{Re} = 0.1$ ) has been shown to be small enough for (9) to apply for slit-like channels [15], and it is expected to apply in the present case as well.

Table I shows the value of the apparent viscosity factor  $\mu_{\text{eff}} / \mu$  for the rectangular expansion-contraction compared with corresponding values for a uniform channel and slit-like channels [15] at the same values of  $K$ ,  $S$ ,  $B$ ,  $Sc$ ,  $\text{Re}$ . A value of apparent viscosity for the rectangular expansion-contraction is not yet available for  $\text{Re} = 0.01$ , but will be determined in further development of this work. The factor  $\mu_{\text{eff}} / \mu$  is independent of Reynolds number for uniform channels in fully developed flow.

TABLE I  
APPARENT VISCOSITY/PHYSICAL VISCOSITY RATIO ( $K = 4$ ,  $S = 8$ )

Channel	$\text{Re} = 0.1$	$\text{Re} = 0.01$
rectangular, expansion-contraction	1.15	–
rectangular, uniform	1.18	1.18
slit-like, expansion-contraction	1.04	1.15
slit-like, uniform	1.13	1.13

The table shows that, for the current parameter values, the apparent viscosity factor for the rectangular expansion-contraction when  $\text{Re} = 0.1$  is close to the factor for a rectangular channel of uniform cross-section. It is also very close to the value for a uniform slit, but is significantly greater than that for a slit-like expansion-contraction at this Reynolds number ( $\text{Re} = 0.1$ ). For slit-like channels, the apparent viscosities for the expansion-contraction and the uniform channel are close when  $\text{Re} = 0.01$  for the electrokinetic current parameter values, but the apparent viscosity for the expansion-contraction is closer to the physical viscosity when  $\text{Re} = 0.1$ : the reasons for this are discussed by the authors in [15]. This result suggests that the apparent viscosity for an

expansion-contraction increases as the Reynolds number decreases, in which case  $\mu_{\text{eff}} / \mu$  for the rectangular expansion-contraction may become significantly greater than the value 1.18 for a uniform rectangular channel. This will be explored in further work on this topic.

#### ACKNOWLEDGMENT

This research was supported by the Australian Research Council Grants Scheme.

#### REFERENCES

- [1] G. Whitesides and A. Stroock, "Flexible methods for microfluidics," *Phys. Fluids*, vol. 54, no. 6, pp. 42–48, 2001.
- [2] M. Gad-El-Hak (ed.), *The MEMS Handbook*, second edition, CRC Press, Boca Raton, 2006.
- [3] H. A. Stone and S. Kim, "Microfluidics: basic issues, applications, and challenges," *AIChE J.*, vol. 47, No. 6, pp. 1250–1254, 2001.
- [4] H. A. Stone, A.D. Stroock and A. Ajdari, "Engineering flows in small devices: microfluidics towards a lab-on-a-chip," *Annu. Rev. Fluid Mech.*, vol. 36, pp. 381–411, 2004.
- [5] D. Li, *Electrokinetics in Microfluidics*. Interface Science and Technology, Vol. 2 (ed. A. Hibbard), Academic Press, 2004.
- [6] R.J. Hunter, *Zeta Potential in Colloid Science: Principles and Application*. Academic Press, New York, 1981.
- [7] G.M. Mala, D. Li and J.D. Dale, "Heat transfer and fluid flow in microchannels," *Int. J. Heat Mass Transfer*, vol. 40, pp. 3079–3088, 1997.
- [8] G.M. Mala, D. Li, C. Werner and H. Jacobasch, "Flow characteristics of water through a microchannel between two parallel plates with electrokinetic effects," *Int. J. Heat and Fluid Flow*, vol. 18, no. 5, pp. 489–496, 1997.
- [9] M. Chun and H.W. Kwak, "Electrokinetic flow and electroviscous effect in a charged slit-like microfluidic channel with nonlinear Poisson-Boltzmann field," *Korea-Australia Rheology J.*, vol. 15, no. 2, pp. 83–90, 2003.
- [10] W.R. Bowen and F. Jenner, "Electroviscous effects in charged capillaries," *J. Coll. Interface Sci.*, vol. 173, pp. 388–395, 1995.
- [11] D. Brutin and L. Tadrist, "Modeling of surface-fluid electrokinetic coupling on the laminar flow friction factor in microtubes," *Microscale Thermophysical Engineering*, vol.9, pp. 33–48, 2005.
- [12] J. Hsu, C. Kao, S. Tseng, and C. Chen, "Electrokinetic flow through an elliptical microchannel: Effects of aspect ratio and electrical boundary conditions," *J. Coll. Interface Sci.*, vol. 248, pp. 176–184, 2002.
- [13] L. Ren, D. Li and W. Qu, "Electro-viscous effects on liquid flow in microchannels," *J. Coll. Interface Sci.*, vol. 233, pp. 12–22, 2001.
- [14] D. Li, "Electro-viscous effects on pressure-driven liquid flow in microchannels," *Colloids and Surfaces A*, vol. 195, pp. 35–57, 2001.
- [15] M.R. Davidson and D.J.E. Harvie, "Electroviscous effects in low Reynolds number liquid flow through a slit-like microfluidic contraction," *Chem. Eng. Sci.*, vol. 62, pp. 4229–4240, 2007.
- [16] M.R. Davidson, D.J.E. Harvie and P. Liovic, "Electrokinetic flow resistance in pressure-driven liquid flow through a slit-like microfluidic contraction," in *Proc. 16<sup>th</sup> Australasian Fluid Mechanics Conf.*, Gold Coast, Australia, 2-7 Dec. 2007, pp. 798–802.
- [17] R.P. Bharti, D.J.E. Harvie and M.R. Davidson, "Steady flow of ionic liquid through a cylindrical microfluidic contraction-expansion pipe: Electroviscous effects and pressure drop," *Chem. Eng. Sci.*, accepted for publication.
- [18] M. Rudman, "A volume-tracking method for incompressible multifluid flows with large density variations," *Int. J. for Numerical Methods in Fluids*, vol. 28, pp. 357–378, 1998.
- [19] D.J.E Harvie, M.R. Davidson, J.J. Cooper-White and M. Rudman, "A parametric study of droplet deformation through a microfluidic contraction: Shear thinning liquids," *Int. J. Multiphase Flow*, vol. 33, pp. 545–556, 2007.
- [20] P.Liovic, D.Lakehal, "Multi-physics treatment in the vicinity of arbitrarily deformable gas-liquid interfaces," *J. Comput. Phys.*, vol. 222, pp. 504-535, 2007.